EROSIVE-CORROSIVE WEAR IN STEAM-EXTRACTION LINES OF POWER PLANTS

by

HUNG VIET VU

S.B., University of Washington
(1979)

SUBMITTED TO THE DEPARTMENT OF
MECHANICAL ENGINEERING IN PARTIAL
FULFILLMENT OF THE
REQUIREMENTS FOR THE
DEGREE OF

MASTER OF SCIENCE

at the

MASSACHUSETTS INSTITUTE OF TECHNOLOGY

June 1982

Signature of Author . . . . . .
Department of Mechanical Engineering, May 19, 1982

Certified by . . . . . .
Peter Griffith, Thesis Supervisor

Certified by . . . . . .
Ernest Rabinowicz, Thesis Supervisor

Accepted by . . . . . .
Warren M. Rohsenow, Chairman, Department Graduate Committee

EROSIVE-CORROSIVE WEAR IN STEAM-EXTRACTION LINES OF POWER PLANTS

by

HUNG VIET VU.

Submitted to the Department of Mechanical Engineering on May 19, 1982 in partial fulfillment of the requirements for the Degree of Master of Science

ABSTRACT

Two distinct mechanisms of oxide removal are found in steam extraction lines of the nuclear power plant, Pilgrim 1. Along with the wear data of the plant, the results from the two-phase flow experiment reveal two mechanisms: Erosion on the outside by drop impingement on magnetite, and corrosion on the inside by magnetite dissolution into the flowing water film. In a bend of a complicated steam line, drops always impinge on the outside and water film always flows on the inside. The maximum drop deposition rate occurs on the outside at 60° to 80° for the last elbow of steam line E-103A. In general, the exact point of maximum wear is not known. The local turbulence, which involves separation-circulation occuring on the inside of the 90° elbow after the mid-point, increases the corrosion rate. Changes are recommended to mitigate the wear problem.

Thesis Supervisors: Peter Griffith
Ernest Rabinowicz

Title: Professors of Mechanical Engineering

TO MY PARENTS AND FAMILY

ACKNOWLEDGEMENTS

I would like to take this opportunity to express my appreciation to Professor Peter Griffith for his invaluable guidance, advice and support throughout this research. I would also like to express my gratitude to Professor Rabinowicz for his highly valuable counsel.

Also, I would like to thank Luis E. Sanchez-Caldera whose contribution in this work as a co-investigator is inestimable.

Many thanks to Mr. Don Wassmouth, Mr. Fred Johnson, Mr. Tiny Caloggero and especially to Mr. Bill Finley for their technical assistance. I also would like to thank the many people in the Heat Transfer Lab who gave helpful suggestions now and then.

Special thanks to Ms. Prudy Young for her typing of this thesis.

This project was funded mainly by Boston Edison Company and partially by Duke Power Company.

TABLE OF CONTENTS

	PAGE
TITLE PAGE	1
ABSTRACT	2
ACKNOWLEDGEMENTS	4
LIST OF FIGURES	7
NOMENCLATURE	8
CHAPTER 1. INTRODUCTION	9
1.1 Statement of Problem	9
1.2 Statement of Purpose	9
CHAPTER 2. TWO-PHASE FLOW EXPERIMENT	11
2.1 Introduction	11
2.2 Flow Similarity	11
2.3 Experimental Set-up	13
2.4 Two-Phase Flow Velocity	15
2.5 Visual Flow Studies - Flow Around 90° Elbows	15
2.6 Measurement of Drop Deposition	22
2.6.1 Wall Isokinetic Probe	22
2.6.2 Procedure	22
2.6.3 Results	24
CHAPTER 3. DISCUSSION	30
3.1 Wear Distribution	30
3.1.1 Steam line E-103A	30
3.1.2 Steam line E-104B	32

TABLE OF CONTENTS (Cont.)

	PAGE
3.1.3 Steam line E-105A	36
3.2 Influence of Parameters on Erosion-Corrosion	36
3.1.1 Geometry	36
3.1.2 Bend Alloy	37
3.1.3 Temperature	37
CHAPTER 4. CONCLUDING REMARKS	40
4.1 Conclusions	40
4.2 Recommendations	41
APPENDIX A - Isometric Drawings of Steam Lines	43
APPENDIX B - Materials and 100% Power Flow Conditions	47
APPENDIX C - Theories of Erosion and Corrosion	48
APPENDIX D - Test Equipment Specifications	51

LIST OF FIGURES

FIGURE		PAGE
1	Experimental Set-up	14
2	Isometric Drawing of Test Section	14
3	Calibration Curve for Two-Phase Flow Velocity	16
4	Secondary Flow in Bend	18
5	Photograph of First Elbow (horizontal) Showing Local Turbulence and Distribution of Drops and Water Film	19
6	Photograph of Next-to-Last Elbow (horizontal) Showing Local Turbulence and Distribution of Drops and Water Film	20
7	Photograph of Last Elbow (vertical) Showing Local Turbulence and Distribution of Drops and Water Film	21
8	Wall Isokinetic Probe	23
9	Vacuum Pressure for Annulus	25
10	Vacuum Pressure for Central Tube	26
11	Development of Surface of a 90° Elbow	28
12	Drop Deposition on the Wall of Last Elbow of Test Section	29
13	Wear Pattern in Last Elbow of Steam Line E-103A	31
14	Locations of Thickness Measurement on the Elbow of Steam line E-104B and E-105A	33
15	Wear Pattern in Next-to-Last Elbow of Steam Line E-104B	34
16	Wear Pattern in Last Elbow of Steam Line E-105A	35
17	Corrosion-Temperature Curve	38
A.1	Steam-extraction line E-103A	44
A.2	Steam-extraction line E-104B	45
A.3	Steam-extraction line E-105A	46

NOMENCLATURE

D	Bend diameter
g	Gravity
R	Radius of centerline streamline
V	Gas-liquid mixture velocity
β	Angle around the bend (Fig. 14)
θ	Circumferential angle (Fig. 14)
μ	Viscosity
ρ	Density
σ	Surface tension

Subscripts

f	Liquid
g	Gas

CHAPTER 1

INTRODUCTION

1.1 Statement of Problem

Wet steam lines of many carbon or low-alloy steel power plants, nuclear or conventional, have been reported to suffer severe wear damage. Appreciable amounts of metal loss have been found in bends.

Pilgrim 1 is a nuclear power station owned by Boston Edison. It has had a severe wear problem with some of its steam-extraction lines. Steam-extraction line is a pipe that extracts the steam from the turbine and carries it to the feed-water heater. The term steam line will be used for briefness. Excessive amounts of wear have been found in the last and next-to-last bends of these lines.

For the steam lines, E-103A, E-104B and 105A, the isometric drawings are shown in Appendix A, the materials and the flow conditions are shown in Appendix B, and the wear data are shown in Chapter 3. Maximum wear occurs on the inside of some elbows, or takes place on both the inside and the outside of others. One would not expect that a single wear mechanism could possibly cause this peculiar pattern.

1.2 Statement of Purpose

The objectives of this research are:

1. To understand the distribution of wear in a complicated steam line, and then apply the analysis to the steam lines of Pilgrim 1.

2. To determine the location of maximum wear.

3. To recommend means of mitigating the wear problem.

Knowing the location of maximum wear is of great value because the valuable testing time can be significantly reduced. Wear rate prediction is beyond the scope of the present research.

Appendix C shows the literature survey and the general considerations in erosion and corrosion. After the theoretical studies, the solutions for the location of maximum wear and the wear mechanisms were still not found. A two-phase flow experiment was finally decided upon. Along with the existing wear data, the results from the experiment revealed the wear distribution and the wear mechanisms. The location of maximum wear is also estimated.

In this paper, the term erosion is used to describe erosive-corrosive wear when drop impingement is present, whereas corrosion is specified to be erosive-corrosive wear when liquid-flow assists in metal removal but with no drop impingement occurring. Also, in this paper the following terms are used interchangeably: (a) elbow and bend, (b) inner wall and inside, (c) outer wall and outside.

CHAPTER 2

TWO-PHASE FLOW EXPERIMENT

2.1 Introduction

The steam lines of Pilgrim 1 are complicated piping systems with many closely spaced 90° elbows. The maximum wear of the steam line network occured in the last elbow of steam line E-103A (the isometric drawing of this steam line is shown in Fig. A1).

A scale model of the piping section that includes the three elbows leading to heater E-102A has been constructed for this investigation. Air and water are fluids used in the equivalent two-phase flow. The experiment is concerned mainly with the visual flow studies and drop deposition measurements.

2.2 Flow Similarity

Besides geometric similarity, six independent groups are, in general, necessary to describe a two-phase flow in an adiabatic system. A perfect scaling of a two-phase flow experiment would include geometric similarity and the following dimensionless groups:

1. Density ratio $\frac{\rho_f}{\rho_g}$
2. Viscosity ratio $\frac{\mu_f}{\mu_g}$
3. Weber number $We = \frac{\rho_g V^2 D}{\sigma}$
4. Reynolds number $Re = \frac{\rho_f V D}{\mu_f}$
5. Quality x

6. Modified Froude number $Fr^* = \frac{\rho_f}{\rho_g} \frac{V^2}{gD}$

For the slow regime that exits in the steam line, E-103A, the dimensionless group that is most important is the modified Froude number. Nevertheless, if Fr* is the same in the model and application, entrainment will be too low. If, on the other hand, entrainment is to be kept the same, velocity will be too high for Fr*. Table 1 shows the flow conditions for the actual steam line and the experiment. The compromise velocity for the air-water experiment is 115 ft/s, and the corresponding entrainment is 25%.

Table 1. Flow Conditions for Actual Steam Line and Air-Water Experiment

		Actual	Experiment
Temperature	T	196°F	80°F
Pressure	p	63 psia	14.7 psia
Liquid		Water	Water
Gas		Steam	Air
Quality	x	0.93	0.93
Pipe diameter	I.D.	1.9375 ft	1.1667 ft
Average velocity	V	126 ft/s	115 ft/s

Since we are only interested in knowing the results qualitatively in this experiment, most of the scaling laws, including kinematic similarity, for a perfect flow similarity are relaxed.

2.3 Experimental Set-up

The experimental set-up is shown in Fig. 1. (Specifications of the blower and the water flowrater are shown in Appendix D). The entrance pipe is long enough to ensure fully-developed flow conditions. The isometric drawing of the test section is shown in Fig. 2.

One of the important parts in the set-up of this two-phase flow experiment is trying to get the air supplied from the blower with high velocity to get enough entrainment. A small increase in back pressure associated with pressure drop causes a large decrease in the efficiency of the blower. Consequently, the velocity of the air is reduced significantly.

The test section consists of three elbows and four plexiglas tubes all of 2 in. I.D. The R/D is 1.5 for the elbows. The glass elbows are for flow visual studies, whereas the copper elbows are for drop deposition measurements. (Holes can be made much easier in metal than in the glass). The elbows are connected to the pipes by hose connections. These couplings are excellent because changes are so easy. The lip of the coupling is a good simulator of the weld joint in the actual piping. The weld, a single-V groove butt joint, is a potential problem because the local turbulence, induced at the joint, increases considerably dissolution rate.

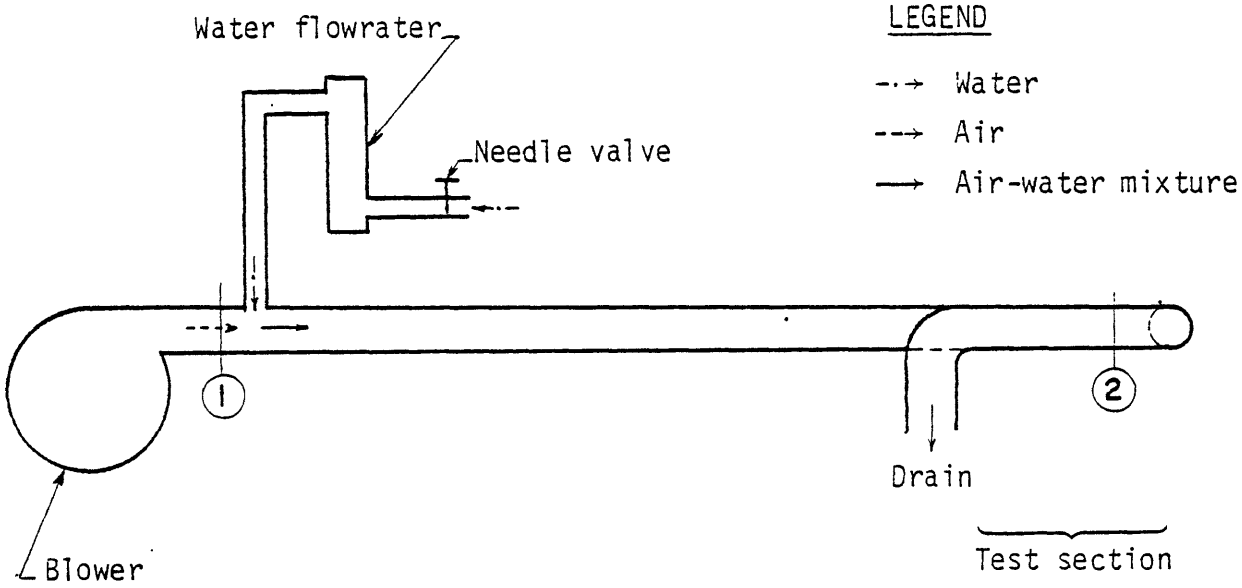

Fig. 1. Experimental Set-up

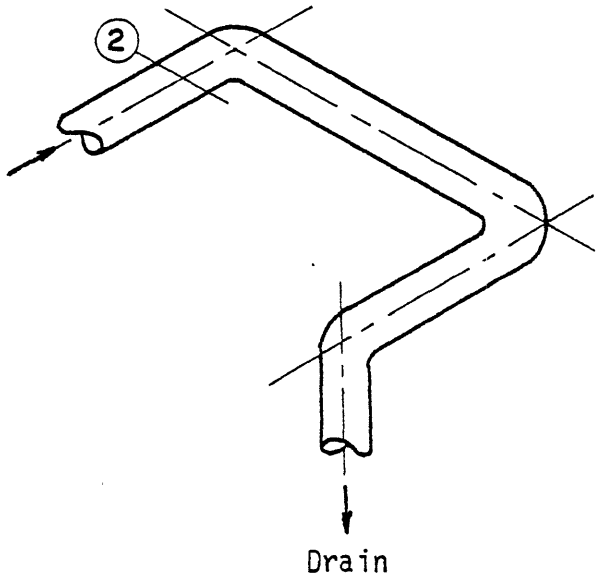

Fig. 2. Isometric drawing of test section

2.4 Two-Phase Flow Velocity

The velocity of a two-phase flow cannot be determined directly by using the pitot tube, but only indirectly by using the calibration curve established from the procedure outlined below.

First, only air was introduced into the test section. By setting the gate valve of the blower at various positions, the range of air flow rates could be obtained. Fig. 1 shows the velocity measurement locations. A curve of the centerline velocity at location 2 versus the centerline velocity at location 1 is plotted in Fig. 3 for the range from closed to fully open for the valve. The appropriate amount of water such as $x = 0.93$, was then introduced into the test section. The mixture velocity can now be determined by using the calibration curve (Fig. 3), if the air velocity at location 1 is known. The velocity of the air-water mixture is slightly lower than that of the air flow alone because of higher pressure drop in the two-phase flow.

During each test run, the superficial velocity of the air was kept at 115 ft/s and that of water was 0.0102 ft/s, for 93% of quality. The water flow rate is 380ml/min.

2.5 Visual Flow Studies - Flow around 90° elbows

Glass elbows together with coloring agent were used for flow visualization. The effect of the secondary flow generated in bends was surprising. When dye is injected at location 1 and if the position is traversed from top to bottom, the effect of entrainment can be seen clearly.

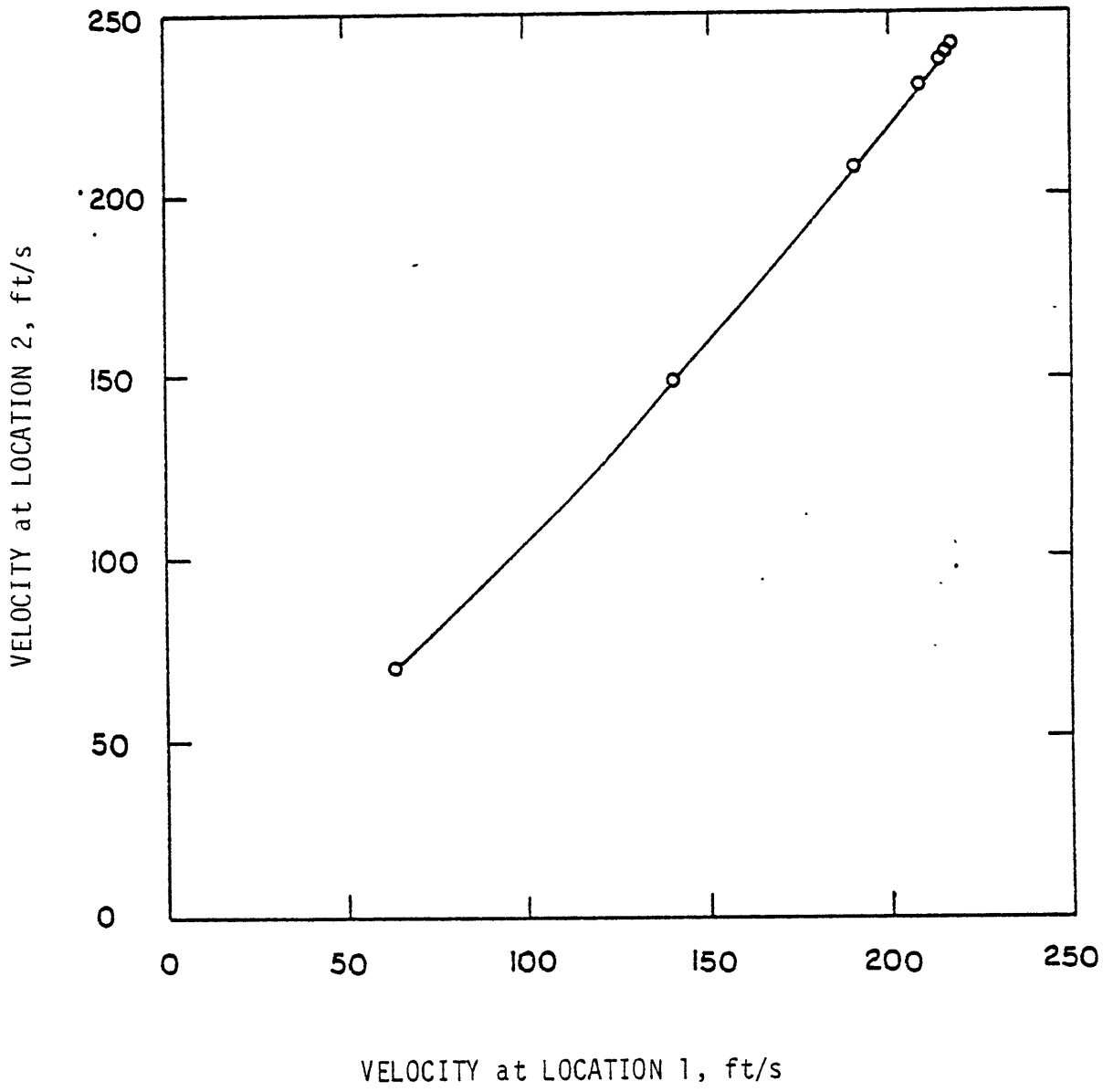

Fig. 3. Calibration curve for two-phase flow velocity.

Flow around a bend induces a double helix perpendicular to the primary flow (Fig. 4). Adjacent to the walls, the fluid flows from the outside to the inside of the bend and in the opposite direction when it flows across the diameter AA. Because the liquid is in the boundary layer, the fluid particles adjacent to the wall move more slowly than the main flow. The resulting centrifugal force is insufficient to balance the pressure gradient induced by the curvature, and the liquid flows to the inside of the bend. Consequently, the gas flows to the outside by continuity.

It was observed that the bend acts as a phase separator. Most of the drops strike the outside of the bend and there is hardly any drop impingement at all on the inside. The drops do not follow the air stream line, but tend to travel on straight lines owing to their greater inertia. Drops are thrown to the outside, then these drops form filaments that spiral to the inside. These spiral paths are the resultant of a streamwise drag force on the filaments by the primary gas flow and a peripheral drag force due to the twin vortices of the secondary flow. The filaments all converge to a region called local turbulence. This local turbulence also involves separation and recirculation.

Figs. 5-7 show the identical distributions of drops and film in all three bends. Drops impinge on the outside while water film flows along the inside. Because of the piping geometry, however, the

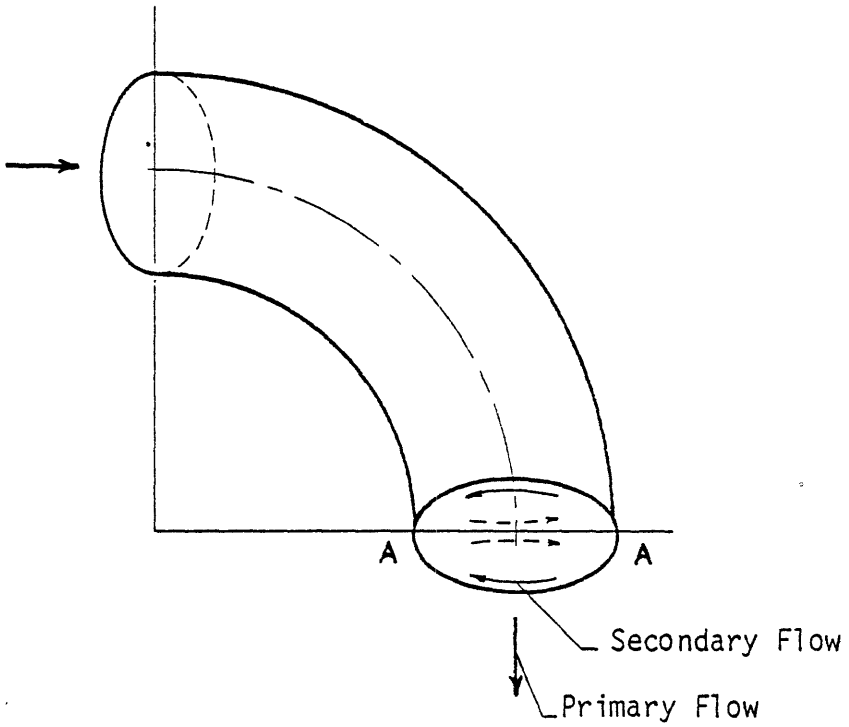

Fig. 4. Secondary flow in bend

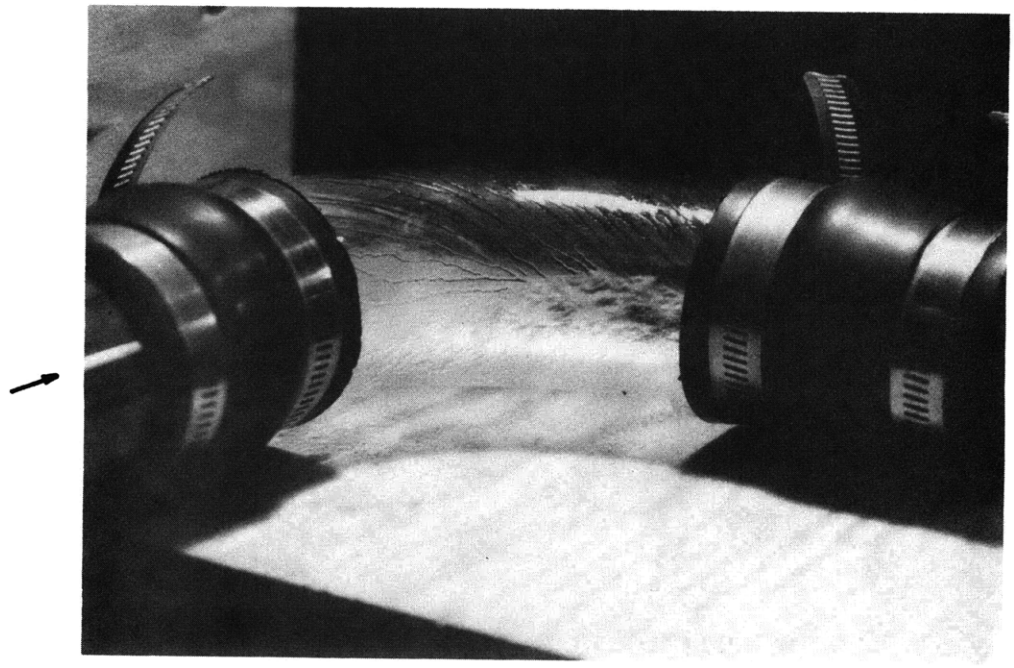

(5a)

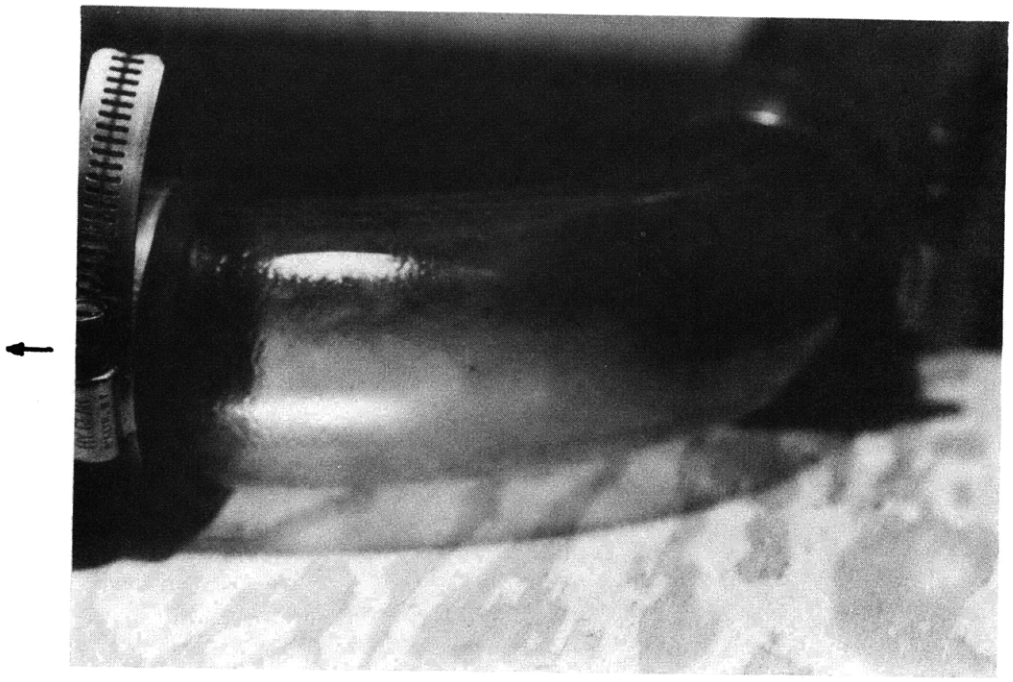

(5b)

Fig. 5. Photograph of first elbow (horizontal) showing local turbulence and distribution of drops and water film: (a) inside, (b) outside.

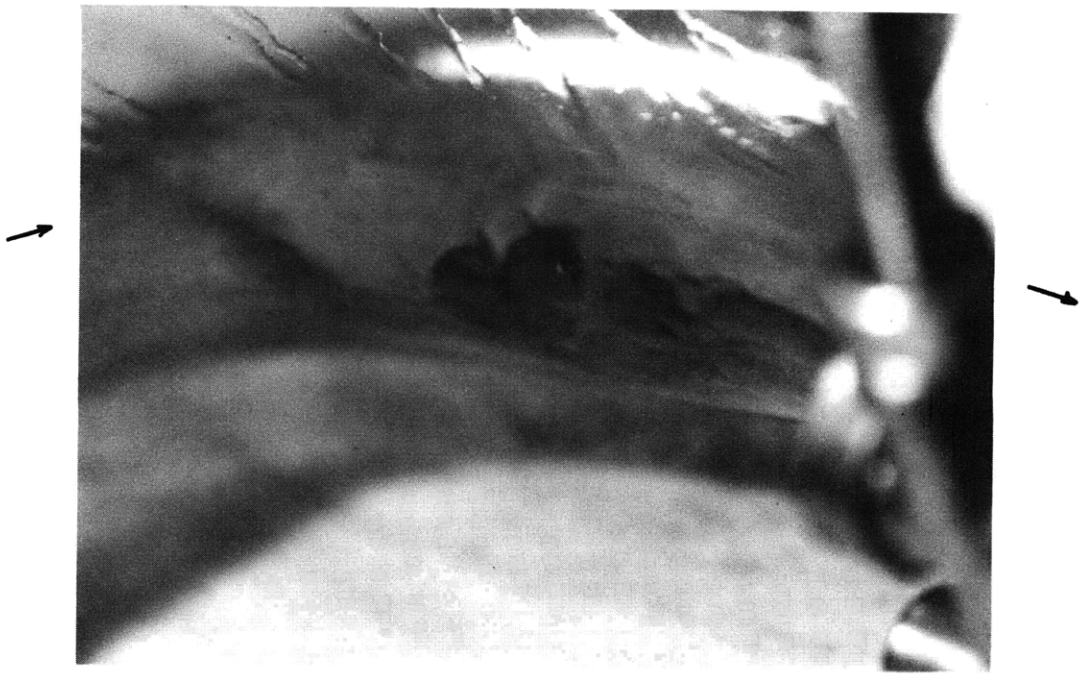

(6a)

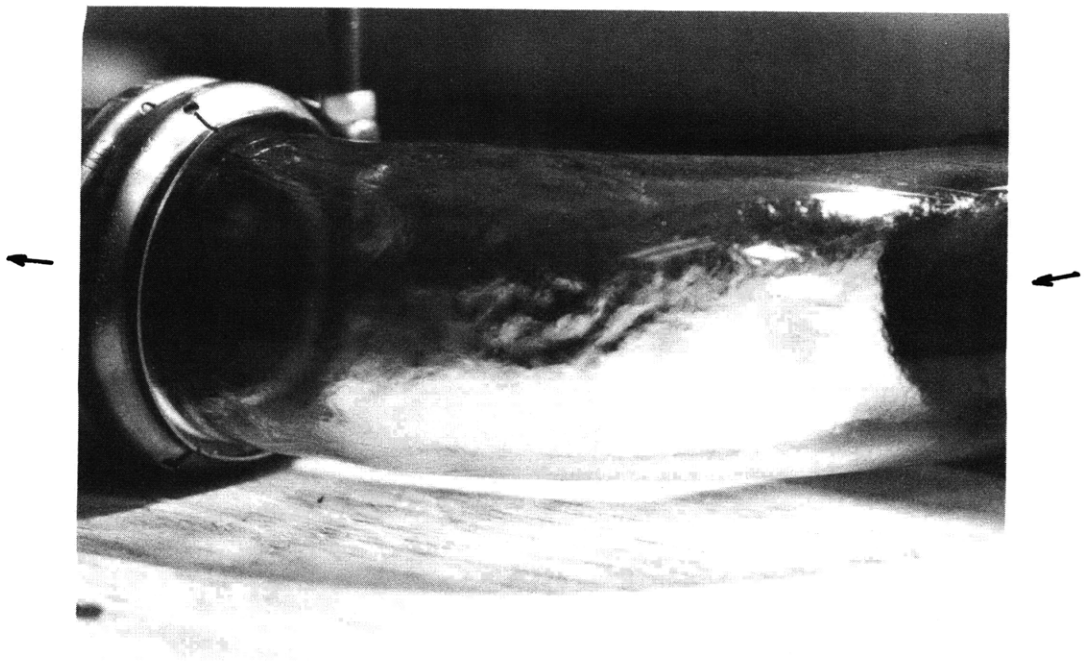

(6b)

Fig. 6. Photograph of next-to-last elbow (horizontal) showing local turbulence and distribution of drops and water film: (a) inside, (b) outside.

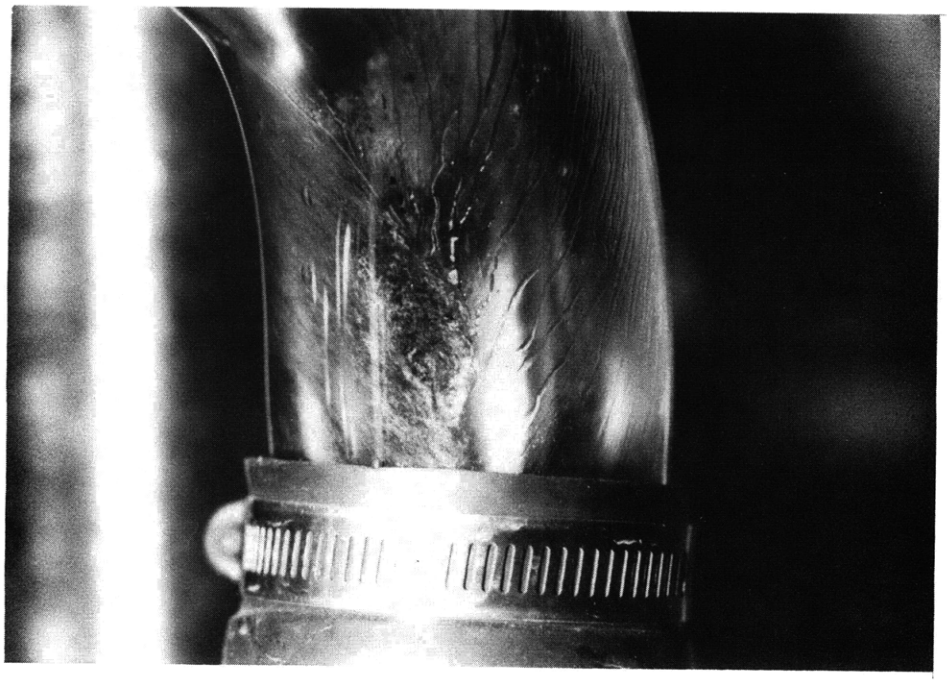

(7a)

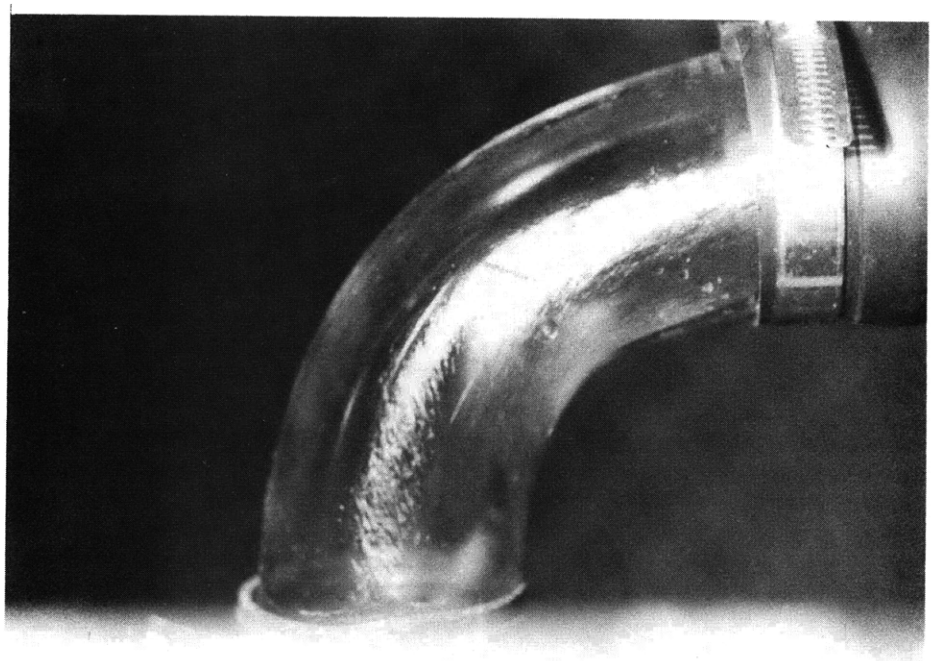

(7b)

Fig. 7. Photograph of last elbow (vertical) showing local turbulence and distribution of drops and water film: (a) inside, (b) outside.

impacting drops are more concentrated in the last elbow.

2.6 Measurement of Drop Deposition

In order to determine the location of maximum wear by drop impingement, we measure the rate of drops deposited on the wall. The last elbow was chosen for the measurements.

2.6.1 Wall Isokinetic Probe

Drop deposition are measured by using a new instrument that is a modified isokinetic probe: a wall isokinetic probe. An isokinetic probe is a well developed device described in the standard texts on two-phase flow (e.g. Hetsroni, 1982). It consists of a pitot tube with suction such that all the drops that would normally impact the probe are collected. The amount of liquid is recorded.

The wall isokinetic probe is an identical device except that is is mounted on the wall. Fig. 8 shows a wall isokinetic probe that has been designed and built. The probe essentially consists of a central tube and an annulus. When mounted flush to the wall, the annulus is used to suck off any liquid film so that the central tube only collects all the drops that would normally strike the wall. The rate of water collected is the rate of drop deposition.

2.6.2 Procedure

Two vacuum pumps were used, one is for the annulus and the other is for the central tube. When both the vacumm pressures are operated in their flat regions, the drops collected by the probe are the

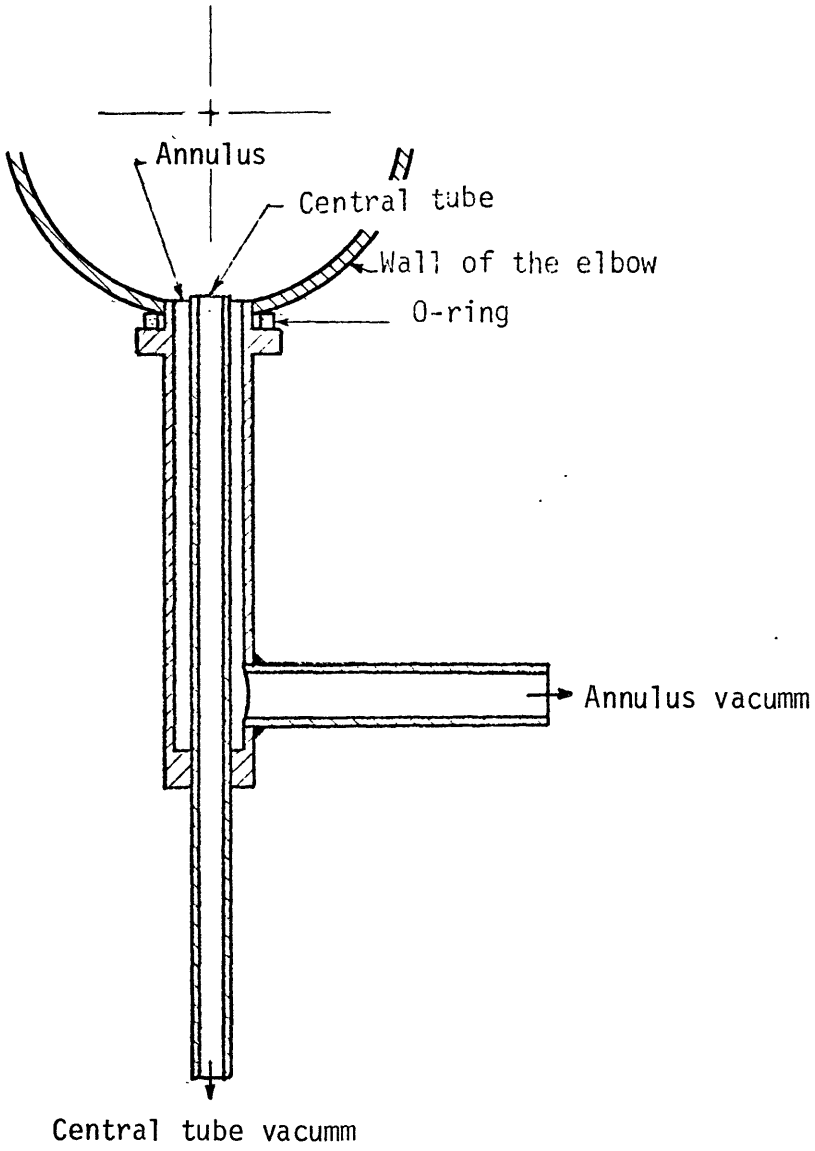

Fig. 8. Wall isokinetic probe
(scale 1 = 1)

actual drops that would impinge the wall. The establishment of these flat regions are shown as follows.

First, a hole was drilled on the outside at 79° around the bend. The probe was inserted and the vacuum pressure was applied to the annulus. The rate of drops, collected through the central tube, is plotted against the annulus vacuum pressure, as shown in Fig. 9. In the flat region of Fig. 10, the rate does not depend on the vacuum pressure (i.e., the probe only collected the drops but not the water film). The vacuum pressure for the central tube was then applied, while the annulus vacumm pressure was kept at a constant value in the flat region of Fig. 9. The rate of drops collected by the probe was then plotted against the central tube vacuum pressure in Fig. 10. After the first hole was plugged flush to the wall (by modelling clay), the next hole was tested. The procedure was repeated until all the measurements were made for all the holes on the bend. During each test run the vacuum pressures for the annulus and the probe were kept at 9 and 7 in. of Hg, respectively. (These values are in the flat regions of Figs. 9 and 10).

2.6.3 Results

When the thickness is measured at a number of evenly distributed locations on the wall of an elbow, it is difficult to represent the wear data on a single two-dimensional plane; because the wall of the elbow is three dimensional. A method has been developed to overcome this difficulty. The elbow is first cut and folded out, with the inside surface facing up, so that the three-dimensional figure becomes a two-

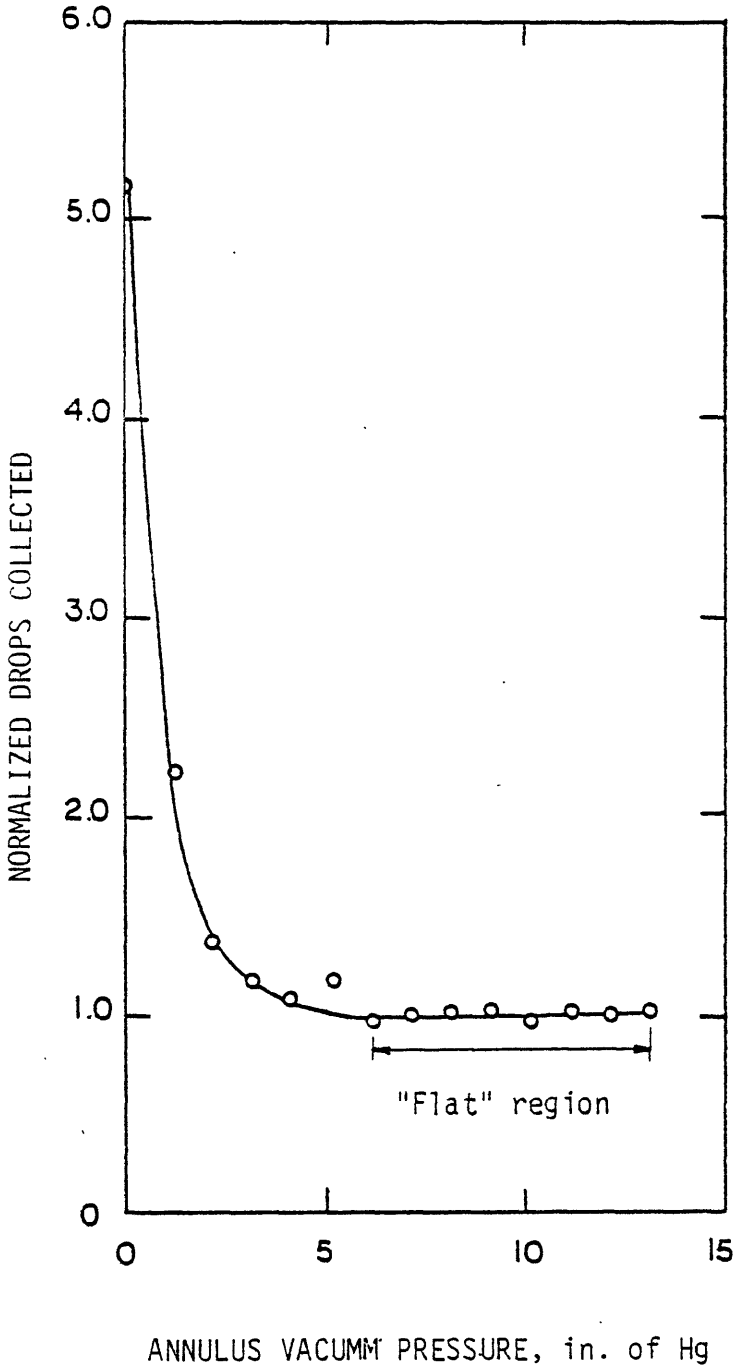

Fig. 9. Vacuum pressure for annulus

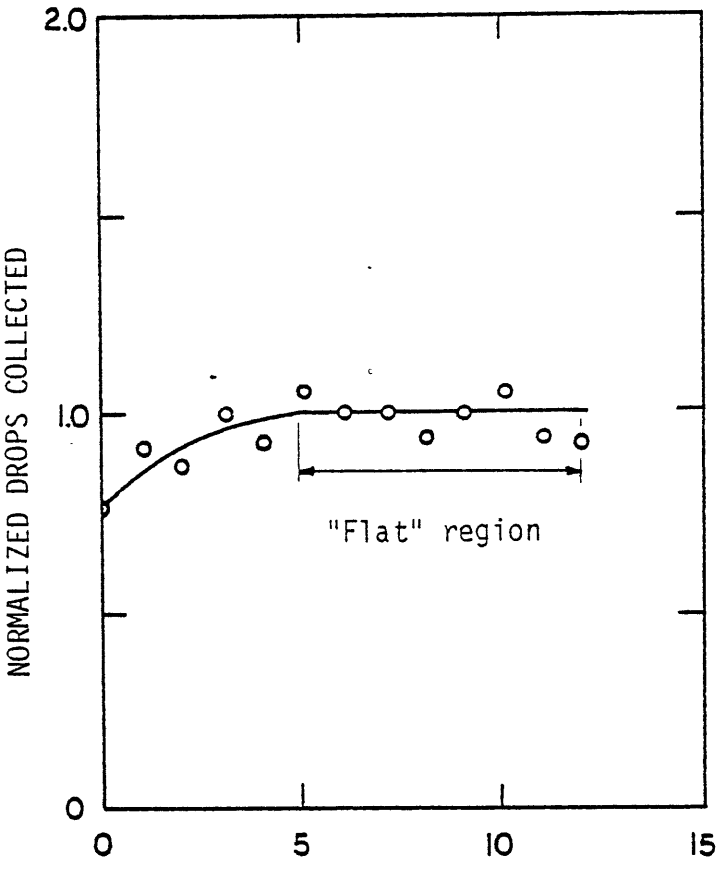

Fig. 10. Vacumm pressure for central tube

dimensional one as shown in Fig. 11. (The number of cutting planes are not restricted, but there are four here for convenience.) This is called "the development of the surface" of an elbow.

The rates of drop deposition on the outside of the last elbow are shown on Fig. 12. The maximum rate of drop deposition occurs on the outside at about 60 to 80° around the bend.

It should be emphasized that the behavior of the water film and the location of the maximum drop deposition rate did not change significantly over a wide range of air-water mixture velocities.

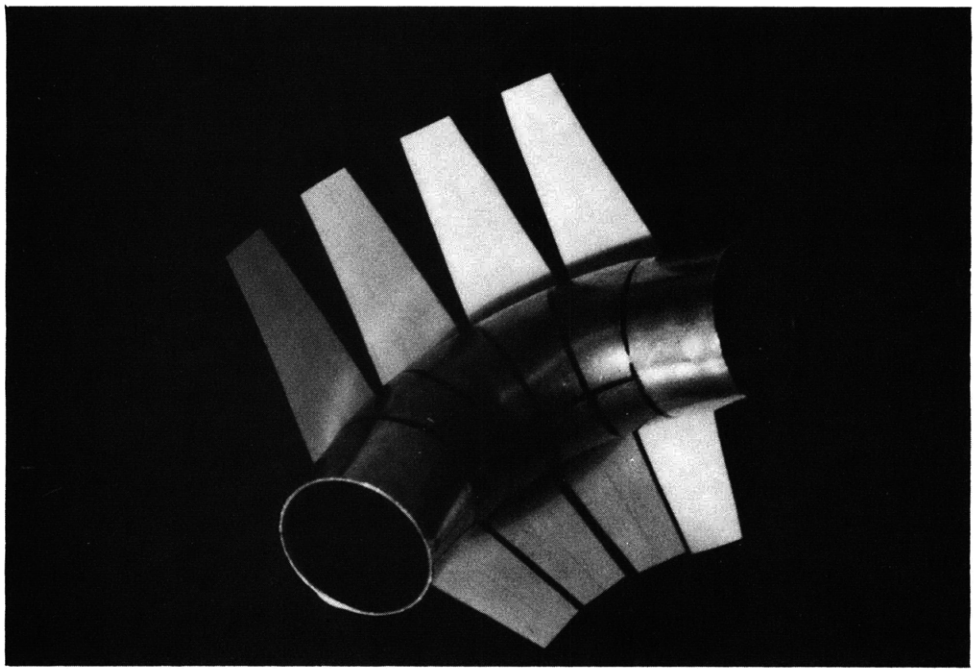

Fig. 11 Development of surface of a 90° elbow

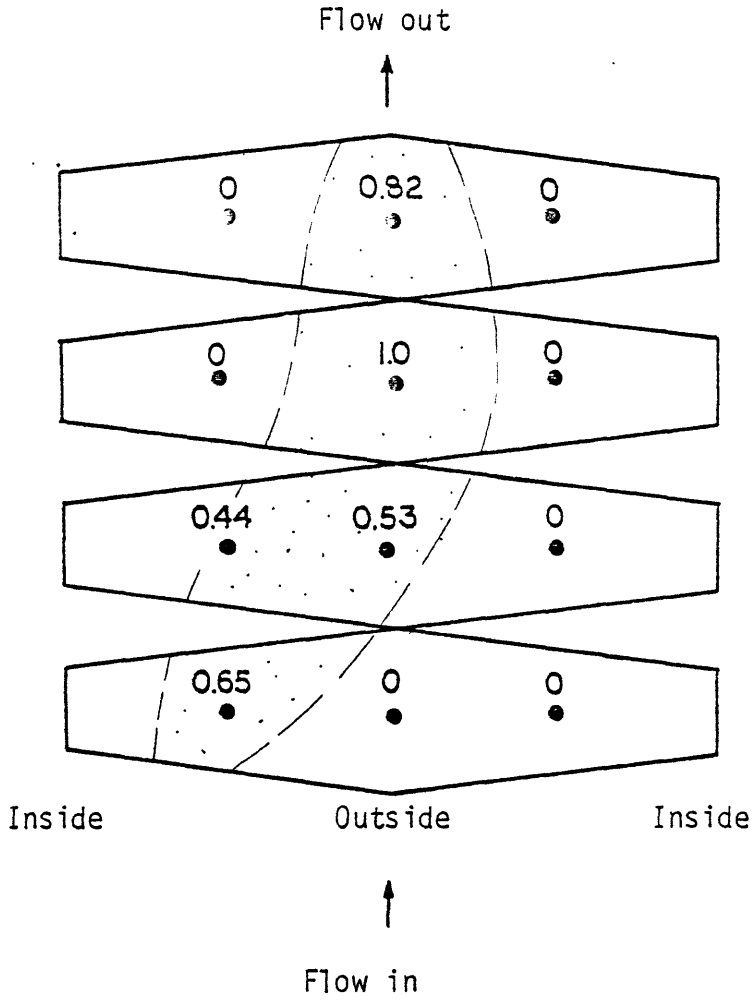

LEGEND

- ● Locations of measurement
- (·) High drop depositing region
  (Normalized data with respect to the maximum deposition)

Fig. 12. Drop deposition on the wall of last elbow of test section

CHAPTER 3

DISCUSSION

The most important wear data of some of the steam lines, taken by Peabody Testing Company using ultrasonic testing, are discussed in this chapter. The wear mechanisms are revealed and the location of maximum wear is estimated. The parameters and their influence on erosion-corrosion are discussed. As a result, recommendations for eliminating the wear problem will be obtained.

3.1 Wear Distribution

The wear patterns presented here are of the following:

1. Last elbow of steam line E-103A
2. Next-to-last elbow of steam line E-104B
3. Last elbow of steam line E-105A

3.1.1 Steam line E-103A

Using the development-of-surface method, the wear pattern of the last elbow is shown in Fig. 13. The wear pattern is represented by the iso-thickness contour lines. The minimum thickness corresponds to the maximum wear. There are mainly two regions of wear: inside and outside. Clearly, corrosion is responsible for the wear on the inside, whereas erosion is responsible for the wear on the outside. In the wear regions, the minimum thickness is 0.248" on the inside and 0.305" on the outside.

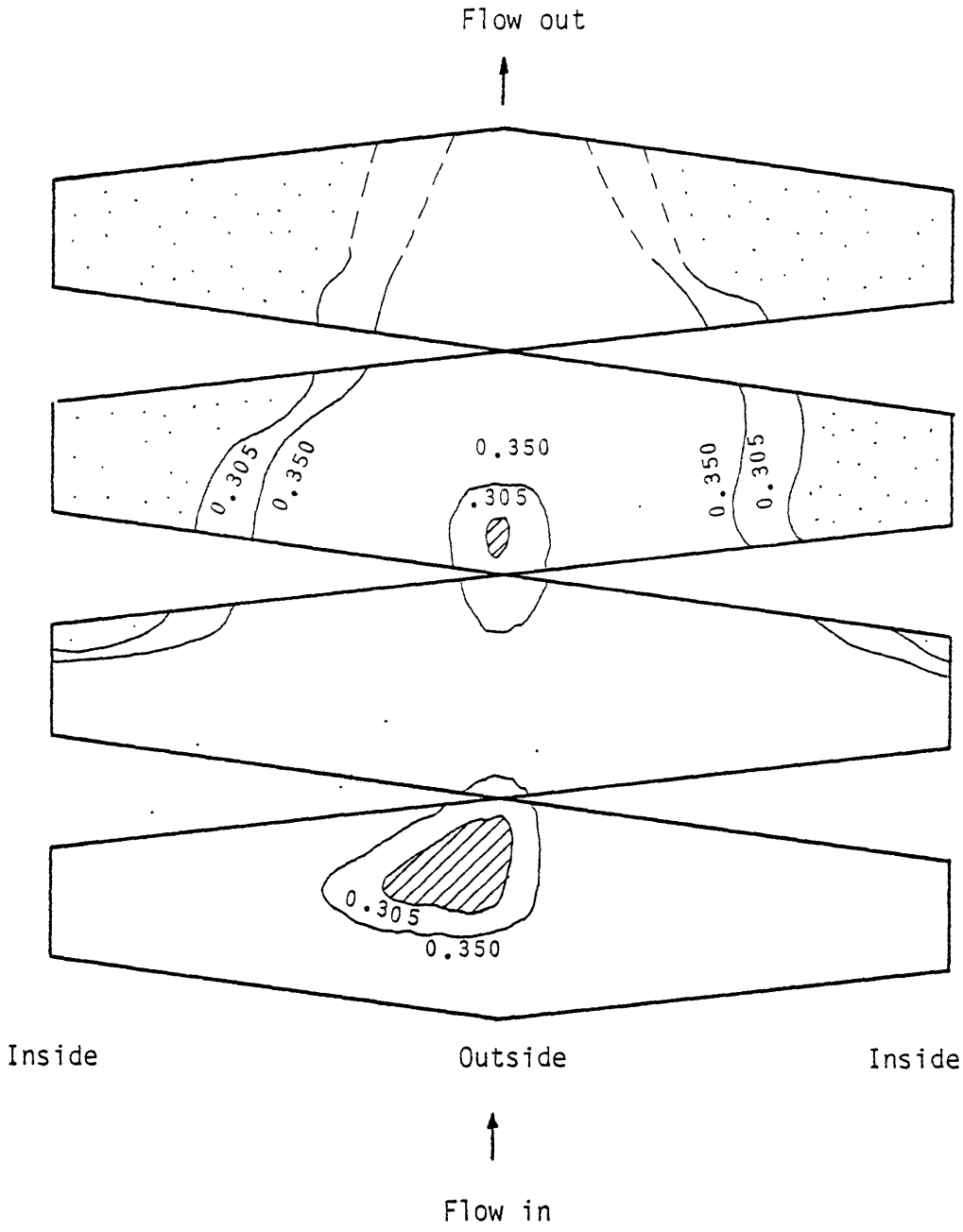

Fig. 13. Wear pattern in last elbow of steam line E-103A (after 9 years in service)

The maximum wear on the inside begins downstream of the mid-point of the bend and spreads out the whole inner wall. The maximum wear on the outside is concentrated on the centerline of the outer wall at 17° and 49° around the bend.

3.1.2 Steam line E-104B

Unlike the case of E-103A, the thickness of the next-to-last elbow of steam line E-104B was measured at three angles around the bend β = 20°, 45° and 75°, as shown in Fig. 14. At each of these angles the thickness was measured clockwise circumferentially when facing in the direction of the flow. This circumferential angle is designated by θ.

The wear pattern of this elbow can be represented more straightforwards. It is unnecessary to use the development-of-surface method in this case. The thickness is simply plotted against the circumferential angle θ.

Fig. 15 shows the wear distribution in this next-to-last elbow. There are mainly two regions of wear: inside and outside. Again, corrosion is responsible for the wear on the inside, whereas erosion is responsible for the wear on the outside. The minimum thikcness (or maximum wear) is 0.380".

The wear regions, inside and outside, are not localized; therefore, the exact location of maximum wear of each region is not known.

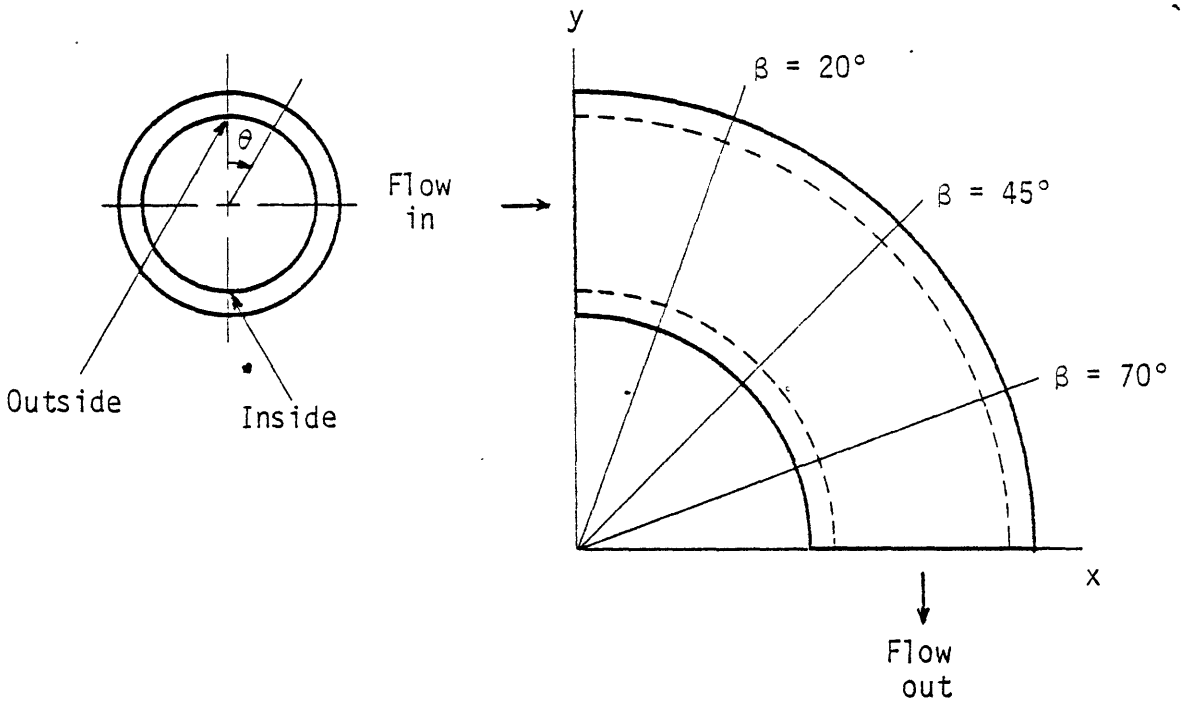

Fig. 14. Locations of thickness measurement on the elbows of steam lines E-104B and E-105A

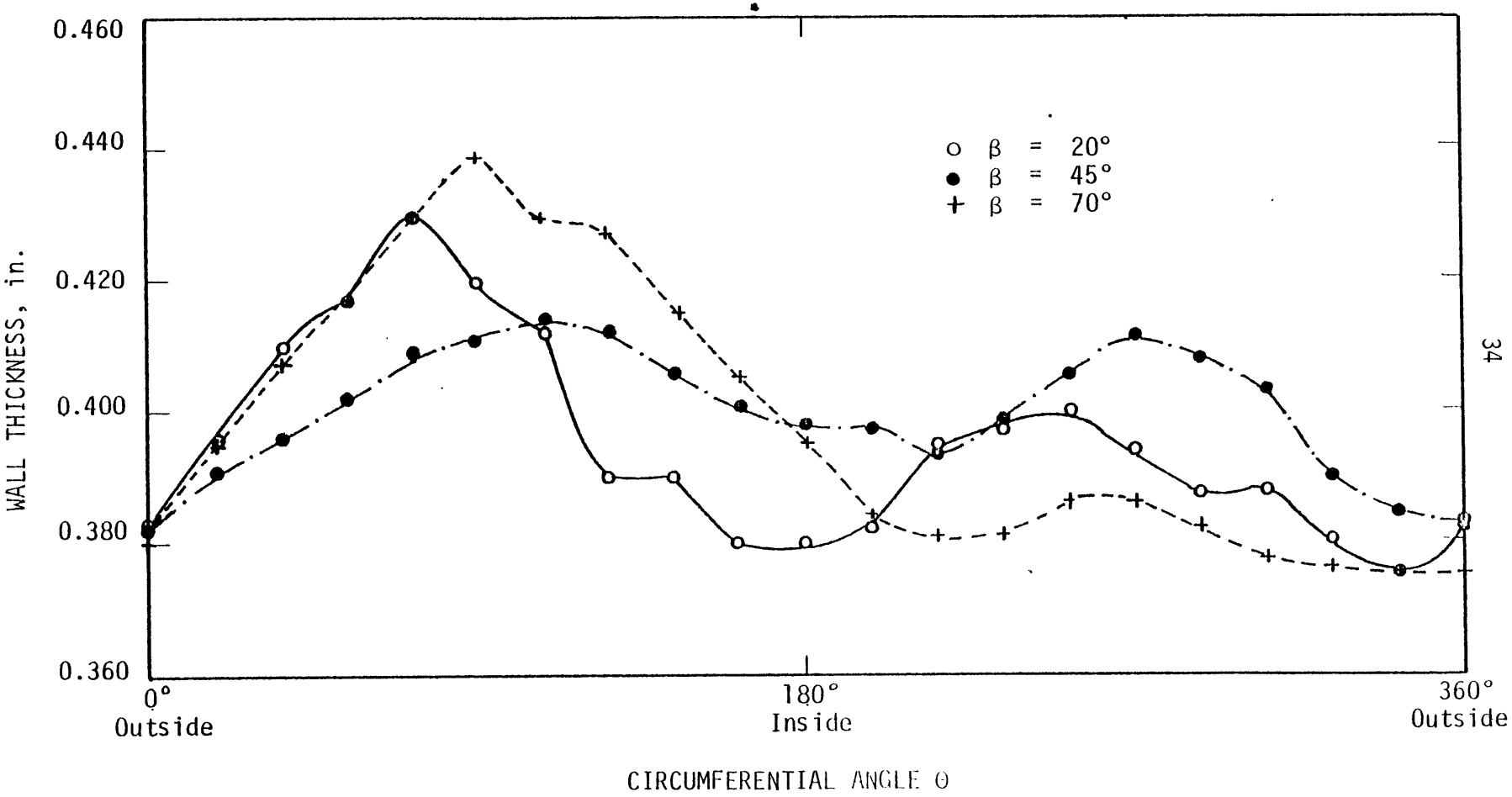

Fig. 15. Wear pattern in next-to-last elbow of steam line E-104B (after 10-1/2 years in service).

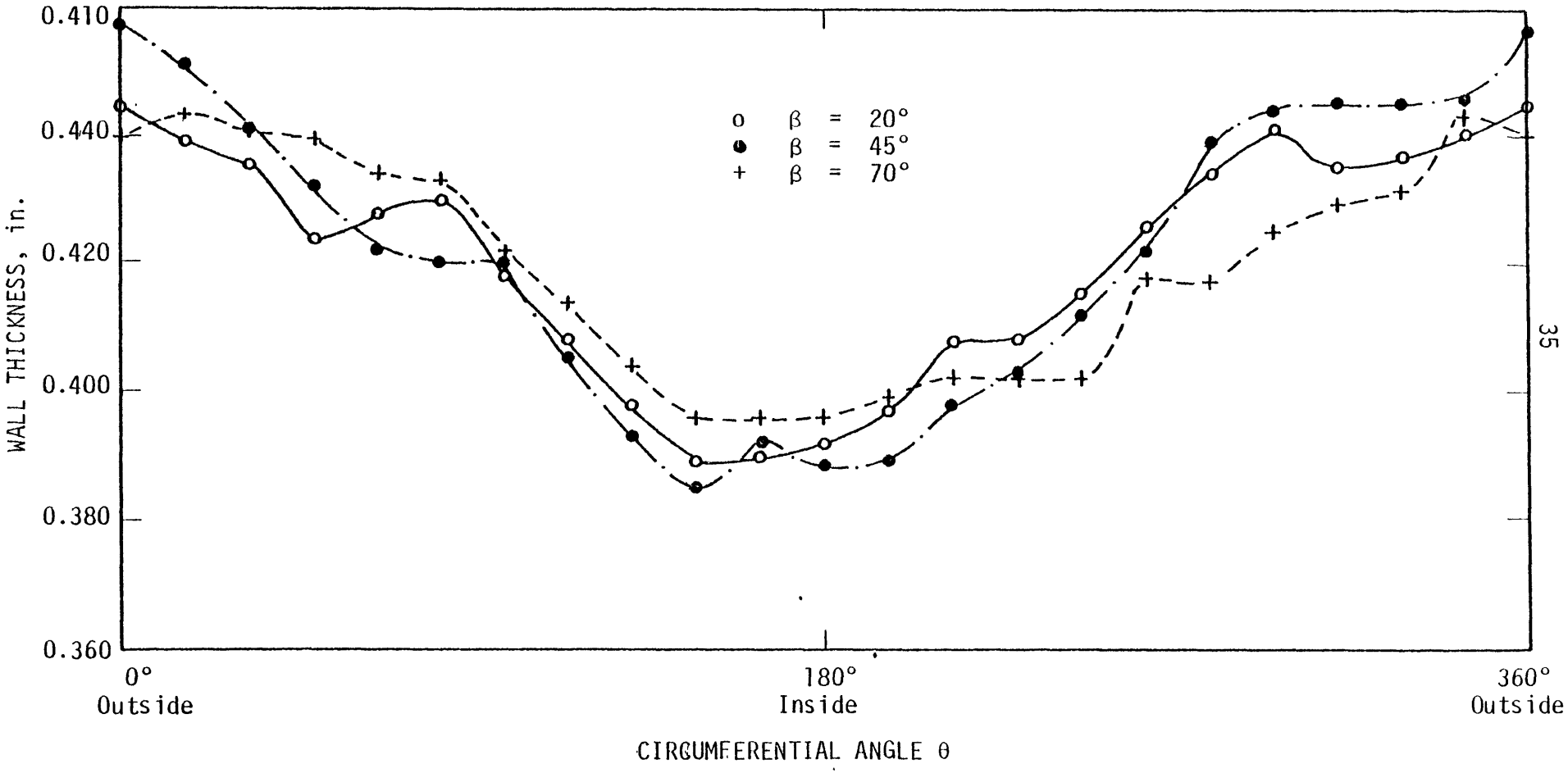

Fig. 16. Wear pattern in last elbow of steam line E-105A (after 10-1/2 years in service).

3.1.3. Steam line E-105A

The thickness of the last elbow of E-105A was measured as in the case of E-104B. Fig. 16 shows the wear distribution in this last elbow. Unlike the case of E-103A or E-104B, there is corrosion domination. The maximum wear of the elbow is only along the inside; the minimum thickness (or maximum wear)is 0.385".

Again, the exact location of maximum wear is not known.

3.2 Influence of Parameters on Erosion-Corrosion

The most important parameters that affect erosion-corrosion are the following:

1. Geometry
2. Bend alloy
3. Temperature

Bignold et al (1981) have reported that high rate of corrosion took place at locations where there is violent fluid turbulence adjacent to the metal surface, either as a result of inherently high fluid velocities or due to the presence of some feature (bend, orifice, etc.) that generates high local turbulence levels.

3.2.1 Geometry

The experimental results showed that the erosion is affected by the geometry of the piping system. It was observed that drop impingement is concentrated on a small area of the last elbow in the test section, whereas the impacted area of the other elbows are much larger.

Although the water film always flows on the inside of the elbows regardless of the elbow orientation the geometry of the bend affects

significantly the corrosion rate. As observed, the local turbulence becomes more violent in a slightly out-of-round bend. This violent local turbulence will increase the corrosion rate.

Fig. 13 shows the last elbow of steam line E-103A has high wear on the outside because of concentrated impacting drops, and also high wear on the inside owing to the bad bend geometry. No satisfactory explanation for the high wear on the outside at 17° around the bend has been found.

3.2.2 Bend Alloy

The bend alloy of steam line E-103A is low-carbon stell A-155 Grade C55 (equivalent to SA-285 Grade C55). This material offers little erosive-corrosive resistance. As a result, the last elbow of E-103A experienced excessive amounts of wear due to both erosion and corrosion.

The bend alloy of steam lines E-104B and E-105A is Yoloy C steel M-531. This material offers higher erosive-corrosive resistance. Similar to E-105A, E-104B suffers a less degree of corrosive damage than E-103A. Unlike E-105A, E-104B experiences erosion because a considerable amount of water is dumped into its line from a moisture separator (not shown in this paper).

3.2.3 Temperature

Keller (1974) has suggested that there exists a temperature at which the maximum corrosion occurs. Below this temperature corrosion rate increases with temperature while above this temperature it decreases with temperature as shown in Fig. 17.

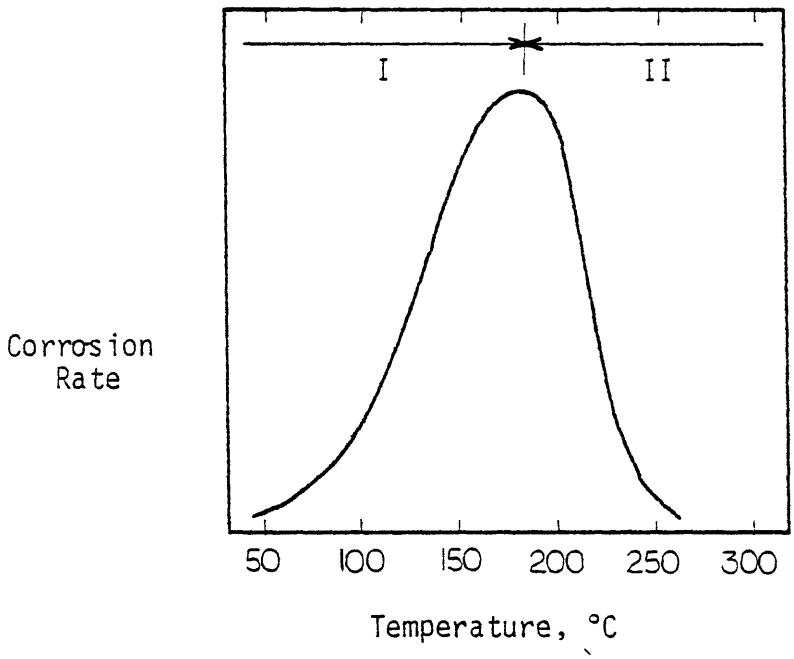

Fig. 17. Corrosion-temperature curve (from Keller, 1974).

The hypothesis is the following. In region I, the ferrous ions, Fe++, extract the hydioxyl ions, OH^-, from water to form the unstable ferrous hydroxide, $Fe(OH)_2$, and release hydrogen via the reaction

$$Fe + 2H_2O \rightarrow Fe(OH)_2 + 2H_2 \quad (1)$$

The speed of the reaction increases with temperature. In this region, the higher the temperature is, the more metal is lost.

At higher temperatures, region II, the ferrous hydroxide quickly decomposes into magnetite (Fe_3O_4) and produces water and hydrogen via the reaction.

$$3Fe(OH)_2 \rightarrow Fe_3O_4 + 2H_2O + H_2 \quad (2)$$

The magnetite layer impedes the dissolution of ferrous ions. Consequently, the rate of corrosion decreases with temperature.

Because of limited test data, Fig. 17 only shows the trend of corrosion-temperature relationship. It has no general validity. Further investigation is needed.

CHAPTER 4

CONCLUDING REMARKS

4.1 Conclusions

As a result of the present investigation, the following conclusions can be made:

1. Drops always impinge on the outside of the bend. They form filaments that then flow rapidly to the inside of the bend. The maximum drop deposition rate occurs on the outside at 60° to 80° around the bend, for the last elbow of steam line E-103A.
2. Secondary flow puts the liquid film, which runs along the bottom of a preceeding horizontal pipe, on the inside of a bend. The violent local turbulence that involves separation and recirculation will occur if the bend is out-of-round or the inner wall is rough. This violent local turbulence increases corrosion rate.
3. There are two distinct wear mechanisms in a bend of a steam line: erosion on the outside by drop impingement on the metal oxide and corrosion on the inside by dissolution of the metal oxide in the flowing water film. Erosion and corrosion are comparable in steam lines E-103A and E-104B, whereas corrosion predominates in steam line E-105A.

4.2 Recommendations

The following items are recommended to mitigate the wear problem in Pilgrim 1:

1. Avoid, if possible, any feature that generates high local turbulence levels.
2. Change the alloy of the bend.
   a) Use more erosion-and corrosion-resistance alloy for steam line E-103A.
   b) Eliminate the water from the moisture separator and use more corrosion-resistance alloy for steam line E-104B.
   c) Use more corrosion-resistance alloy for steam line E-105B.
3. Change the temperature, perhaps by throttling, so that the steam line is no longer operating at the peak in the corrosion rate.

REFERENCES

1. Adler, F. W. (1979) in Treatise on Materials Science and Technology (C.M. Preece, ed.), Vol. 16, pp. 127-178. Academic, New York.

2. Bignold, G. J., K. Garbett, R. Garnsey and I. S. Woolsey (1981), Steam/Water Chemistry Section, Central Electricity Research Laboratories, Leatherhead, Surrey, England.

3. Brunton, J. H., M. C. Rochester (1979), in Treatise on Materials Science and Technology (C.M. Preece, ed.), Vol. 16, pp. 185-249, Academic, New York.

4. Engel, O. G. (1961), Symp. Eros. Cavitat. ASTM STP 307, pp. 3-15. American Society of Testing and Materials, Philadelphia, Pennsylvania.

5. Hetsroni, G. (1982), Handbook of Multiphase Systems, p. 10-7. McGraw-Hill, New York.

6. Heymann, F. J. (1979), "Conclusions from the ASTM Interlaboratory Test Program with Liquid Impact Erosion Facilities," Proc. 5th Int. Conference on Erosion by Solid and Liquid Impact, pp. 20-1 to 20-10.

7. Keller, H. (1979), "Erosion skorrsion an Nabdampfturbinen," VGV, Kraftuerkstechnik, pp. 292-295.

8. Springer, G. (1976), Erosion by Liquid Impact. John Wiley & Sons, New York.

Appendix A

Isometric Drawings of Steam Lines

The isometric drawings of the following steam-extraction lines of Pilgrim 1 are presented here:

E-103A	(Fig. A.1)
E-104B	(Fig. A.2)
E-105A	(Fig. A.3)

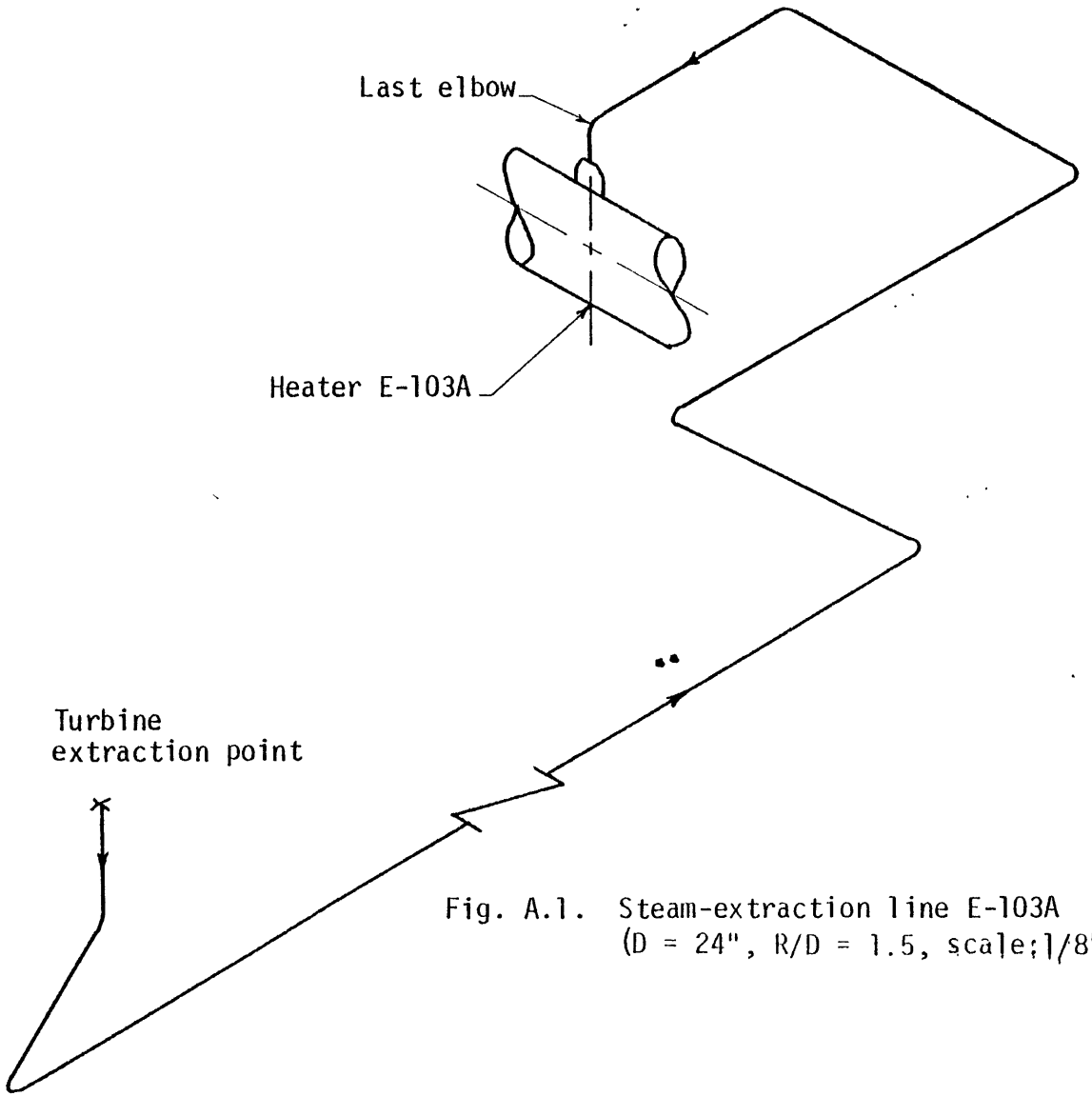

Fig. A.1. Steam-extraction line E-103A
(D = 24", R/D = 1.5, scale;1/8" = 1')

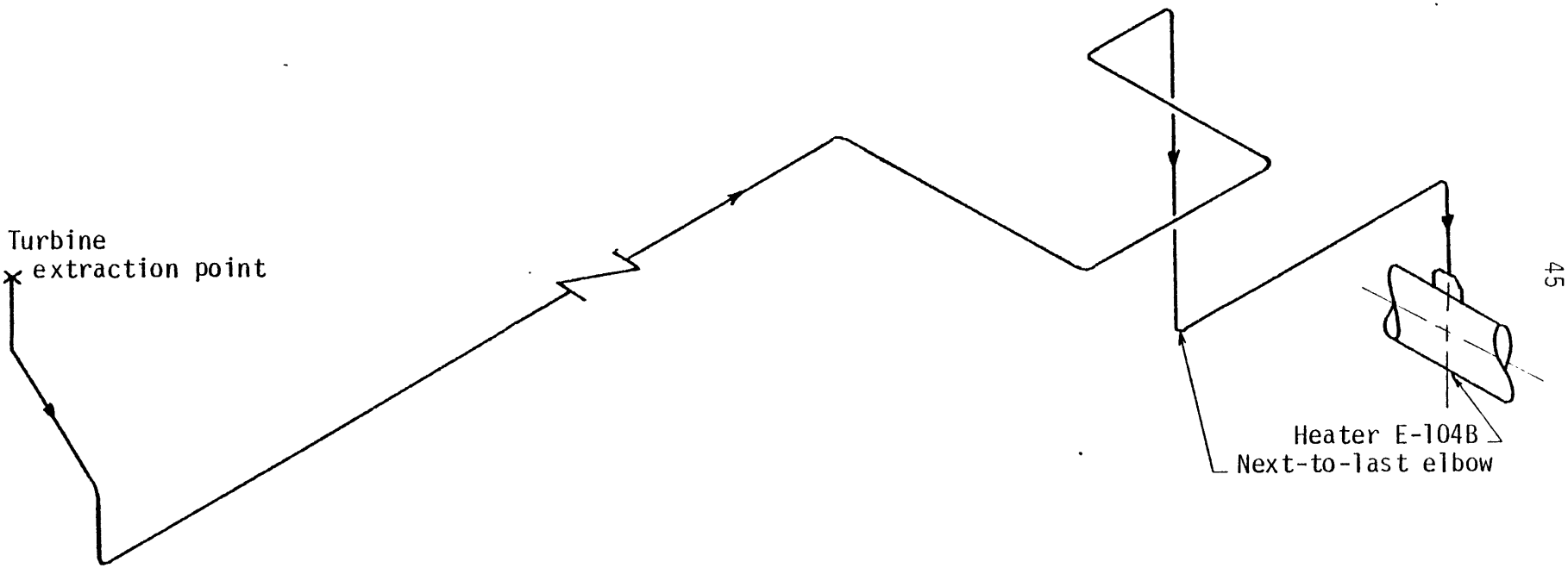

Fig. A.2. Steam-extraction line E-104B
(D = 14", R/D = 1.5, scale: 1/8" = 1')

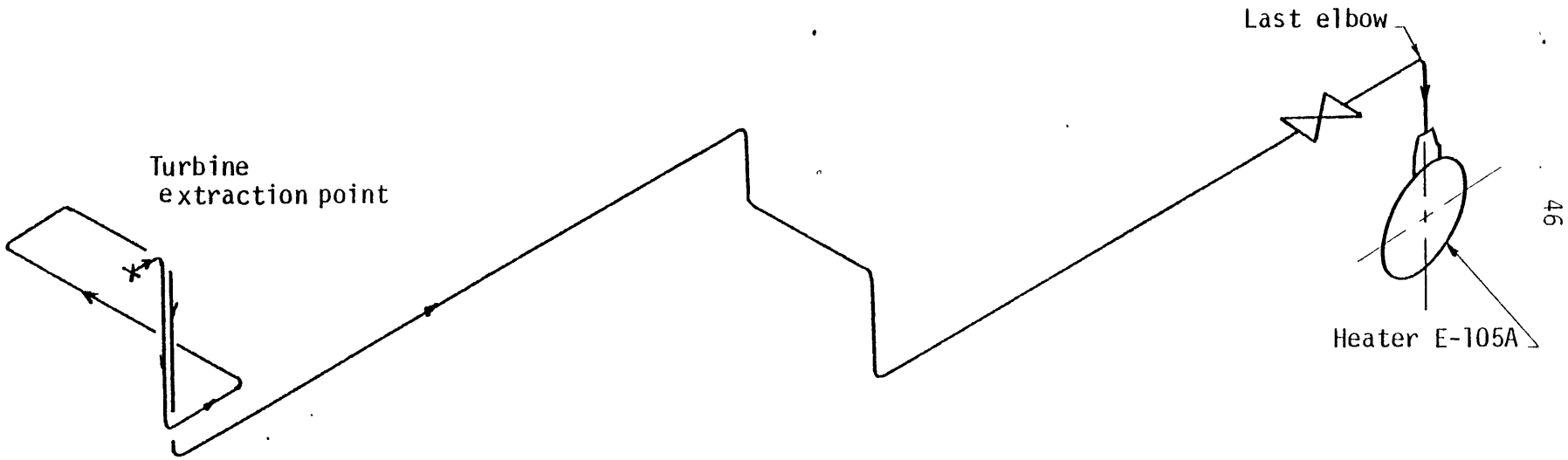

Fig. A.3. Steam extraction line E-105A
(D = 12", R/D = 1.5, scale = 1/8" = 1')

Appendix B

Materials and 100%-power Flow Conditions

Steam line	Material	Flow Rate lb/hr	Temperature °F	Quality
E-103A	Low-Carbon steel A-155 Gr C55 (SA-285 Gr C55)	210086	296.23	0.93
E-104B	Yoloy C steel M - 531	*	327.97	*
E-105A	Yoloy C Steel M - 531	212973	372.95	0.87

*Uncertain

Appendix C

Theories on Erosion and Corrosion

Both erosion and corrosion occur in a wet steam line. Although erosion-corrosion is a widespread problem in steam power plants, not much experimental or theoretical work has been done.

C.1. Erosion

Adler (1979) has described the mechanics of material removal due to liquid impact. Four primary modes of failure were suggested: direct deformation, stress wave propogation, lateral outflow jetting, and hydraulic penetration. Cracks can develop at the boundary of the contact zone, where the tensile stresses are maximum, if produced by direct deformation, or away from the immediate vicinity of the zone as a result of the shock wave generated. The lateral outflow jet can cause great damage when they impact the irregularities because of its significantly higher velocity compared to the impact velocity. Engel (1961) has described that when a lateral outflow jet impacts a protrusion, a shearing stress and a bending moment, produced at the base and the tip of the protrusion, respectively, can lead to metal removal. For a pre-existing crack, the most damaging mode of water drop impact is hydraulic penetration because it can propagate the crack to a much greater extent. After the initiating damage the material removal will finally occur causing the loss of metal upon drop impacts.

Brunton and Rochester (1979) have discussed the drop impinge-

ment erosion of solid surfaces in great detail. The effects of the impact variables and the material properties on erosion are presented in their survey.

Springer (1976) and Heymann (1979) have contributed their models to the theories of erosion. Springer's theory is a cumulative fatigue damage mechanism; Heymann's is an emperical correlation. Although they are great contributions, neither model will give satisfactory results for a wide range of engineering applications because some of the assumptions in Springer's theory are physically unrealistic, whereas Heymann's model may be valid only under the specified test conditions. Other less well-known erosion theories are also available in the literature.

C.2. Corrosion

Corrosion is in part, an electrochemical process involving dissolution and mass transfer of dissolved oxygen and metal when iron (or steel) is in contact with water. (The terminology is confusing; this process is also called erosion-corrosion in literature.) The water film, even very thin, will provide the essential electrotyte for corrosion. Iron loses its materials via either one of the two following idealized processes. Ferrous ions, Fe^{2+}, remove oxygen from water to form iron oxide, Fe_3O_4 (magnetite or ferrous ferrite) and producing hydrogen:

$$3\ Fe + 4\ H_2O \rightarrow Fe_3O_4 + 8H \qquad (C.1)$$

Alternatively, the ferrous ions take hydroxyl ions, OH^-, from water to form ferrous hydroxide, $Fe(OH)_2$, and releasing hydrogen; $Fe(OH)_2$

finally decomposes into magnetite, water and hydrogen:

$$Fe + 2H_2O \rightarrow Fe(OH)_2 + H_2 \qquad (C.2)$$

$$3\ Fe(OH)_2 \rightarrow Fe_3O_4 + 2H_2O + H_2 \qquad (C.3)$$

The rate of metal removal by corrosion is essentially governed by a diffusion-controlled process. The oxide layer, magnetite, formed on the surface may or may not protect the underlying steel depending upon porosity of the magnetite which, in turn, depends on the chemical and hydraulic conditions.

Appendix D

Test Equipment Specifications

Sturtevant Air Compressor

Pressure = 1 psia

Speed = 3500 rpm

Volume = 225 - 400 cfm

Size = 15052

Ship. wt. = 475 lbs

Inlet dia.= 5 in.

Outlet dia. = 5 in.

Motor power rating = 3 hp

Cycle = 60

Voltage = 220 volt

Phase = 3

Water Rotameter

Fisher and Porter Precision Core Flowrater

Tube No. EP-1/4 20-G-5/81

Maximum Flow = 860 ml/min

Model 10A25555

Serves 8106A073341